Shape Factor Estimation and WAG Simulation in Naturally Fractured Reservoirs

Christoph Aublinger
Chair of Reservoir Engineering
University of Leoben

October 2015
Supervisor:
Leonhard Ganzer

Abstract

Naturally fractured reservoirs contain a significant part of the world's remaining oil reserves. A common approach for their simulation is dual porosity modelling. The most significant part in this model is the shape factor that describes the movement of fluids between fracture and matrix domain. Despite decade-long research there is no consensus in the scientific community how the shape factor can be calculated. This thesis uses a single porosity model to estimate the shape factor of a dual porosity model with the same size.

Geological data from Salzburg are used for this thesis. All other necessary input parameters are also given and the way is described how they were obtained. Subsequently, the single porosity and the dual porosity model are presented in detail. It is shown that recovery depends strongly on the driving mechanisms that are taken into account for the simulation. Also relevant is the wettability of the investigated rocks. The injection of gas after water leads to a much higher ultimate recovery than only the injection of water alone. However, ultimate recovery does not depend on wettability. If a correction factor of 1.87 is applied to the equation of Gilman & Kazemi (1973), recovery curves of the single porosity and the dual porosity model are nearly identical for the oil wet case .

Additionally, an algorithm is described that estimates ultimate recovery as a function of the percentage of fractures filled. It is shown that filling of fractures as described in this thesis does only have a small influence on oil recovery. Only the flow rate in the first months of oil production is affected slightly.

Zusammenfassung

Natürlich geklüftete Lagerstätten enthalten einen Großteil der verbliebenen Weltölreserven. Häufig werden diese durch die Dual Porosity Methode simuliert. Der wesentliche Faktor hierbei ist der Shape Factor, jener Parameter, der den Fluss von Fluiden zwischen der Matrix und den Klüften beschreibt. Trotz jahrzehntelanger Forschung herrscht noch immer kein Konsens darüber, wie der Shape Factor berechnet werden kann. In dieser Arbeit wird ein Single Porosity Modell benutzt, um den Shape Factor für ein gleichgroßes Dual Porosity Modell abzuschätzen.

Die benötigten geologischen Daten stammen von einer in Salzburg durchgeführten Feldstudie. Es werden alle weiteren Daten, die für die Simulation benötigt werden, beschrieben, und wie diese ermittelt wurden. Danach werden sowohl das Single Porosity Modell als auch das Dual Porosity Modell detailliert erklärt. Es wird gezeigt, dass die Ölausbeute sehr stark von den in Betracht gezogenen Antriebskräften abhängt. Ebenfalls sehr einflussreich sind die Benetzungseigenschaften der simulierten Gesteine. Eine Injektion von Gas nach einer Injektion von Wasser führt zu einer höheren Endausbeute als die Injektion von Wasser alleine. Die Endausbeute hängt jedoch nicht von Benetzungseigenschaften ab. Wenn man einen Korrekturfaktor von 1.87 auf die Formel von Gilman & Kazemi (1973) anwendet, sind die Ergebnisse des Single Porosity Modells und des Dual Porosity Modells für den hydrophilen Stein nahezu identisch.

Weiters wird ein Algorithmus beschrieben, der die Ölausbeute abschätzt, wenn ein gewisser Prozentsatz der Klüfte gefüllt ist. Es wird gezeigt, dass die Füllung der Klüfe nach der hier beschriebenen Methode nur einen verhältnismaßig geringen Einfluss auf die Ölausbeute hat. Lediglich die Geschwindigkeit der Ölproduktion in den ersten Monaten der Simulation wird geringfügig beeinflusst.

Approval Sheet

This thesis entitled Shape Factor Estimation and Water Alternating Gas Injection in Naturally Fractured Reservoirs prepared and submitted by Christoph Aublinger in partial fulfillment of the requirements for the Degree of Master of Science in Petroleum Engineering has been examined and accepted.

(Leonhard Ganzer)

Declaration

I declare in lieu of oath, that I wrote this thesis and performed the associated research myself, using only the literature cited in this volume.

(Christoph Aublinger)

Contents

Abstract **i**

Zusammenfassung **ii**

Used Notation **ix**

Abbreviations **x**

1 Introduction **1**

2 Background **3**
2.1 Dual Porosity Models 3
2.2 Different Equations for the Shape Factor 4
2.3 Water-Alternating Gas 5

3 Methodology **7**
3.1 NFR Setting/Geological Model 7
3.2 Fracture and Matrix Properties 8
3.3 Single Porosity Model 10
3.4 Dual Porosity Model 12
3.5 Finding Shape Factors 12
3.6 Fracture Filling 12

4 Results **17**
4.1 Sensitivity Analysis Volume Multiplier 17
4.2 Water Injection Only 18
4.3 Water Alternating Gas Simulations 18
4.4 Dual Porosity Simulations 19
4.5 Fracture Filling 20

5 Discussion and Conclusion **26**

A References **28**

B Code for Reference Model **31**

List of Figures

2.1 Dual Porosity Model. 6

3.1 Location of the Study Area. 14
3.2 Geological Outcrop 15
3.3 Single Porosity Model. 15
3.4 Dual Porosity Model. 16
3.5 Principle of Fracture Filling. 16

4.1 Results of VOLMOD Sensitivity Analysis. 21
4.2 Water Injection. 21
4.3 Results for Water Injection Only. 22
4.4 Displacement Induced by Gas Injection. 22
4.5 WAG Injection Only Considering Viscous Driving Forces. 22
4.6 WAG Injection Considering Both Viscous and Capillary Driving Forces. 23
4.7 WAG Injection with Additional Water Injection. 23
4.8 Comparison between Single Porosity and Corrected Dual Porosity Model Oil Wet Rock. 23
4.9 Comparison between Single Porosity and Corrected Dual Porosity Model Water Wet Rock. 24
4.10 Patterns in Oil Saturation. 24
4.11 Recovery Factor if Some Fractures are Filled – Only Viscous Forces. 25
4.12 Recovery Factor if Some Fractures are Filled – Viscous and Capillary Forces. 25

List of Tables

3.1 Reference Case Properties. 9
3.2 Relative Permeability Curves Matrix. 10
3.3 Capillary Pressure Matrix. 11

Acknowledgements

First of all, I would like to express my gratitude to my advisor, Dr. Leonhard Ganzer who provided me with the topic of this thesis and was always available to offer assistance for my questions.

Special thank goes to Nakhon 'Ron' Boonchai for providing me with the geological input for this work.

In addition, I want to thank Tim Berners-Lee, Guido van Rossum and Leslie Lamport. This thesis would not have been possible in the present form without their inventions.

Used Notation

A	m^2	Area
c_f	$\frac{1}{kPa}$	fracture compressibility
c_m	$\frac{1}{kPa}$	matrix compressibility
d	m	distance between area and center of gravitation
$k_{f,eff}$	mD	effective fracture permeability
k_m	mD	matrix permeability
L_x	m	fracture distance in x direction
L_y	m	fracture distance in y direction
L_z	m	fracture distance in z direction
p_f	kPa	fracture pressure
p_m	kPa	matrix pressure
$\hat{q}$	$\frac{m^3}{m^3 sec}$	source term
RF	-	recovery factor
STOIIP	m^3	standard oil initially in placce
μ	Pasec	viscosity
τ	$\frac{1}{sec}$	transfer term
ϕ_f	-	fracture porosity
ϕ_m	-	matrix porosity
σ	$\frac{1}{m^2}$	shape factor

Abbreviations

DFN	Discrete Fracture Network
DP	Dual Porosity
DPDP	Dual Porosity - Dual Permeability
NFR	Naturally Fractured Reservoirs
WAG	Water Alternating Gas

Chapter 1

Introduction

Naturally fractured reservoirs (NFR) contain a significant amount of the world's remaining oil and gas reserves (World Energy Outlook, 2006). Mostly, NFR are associated with brittle rocks (i.e. with carbonate rocks). However, there are also authors who argue that all sedimentary rock reservoirs contain natural fractures to some extent (Nelson, 2001; Narr, Schechter & Thompson 2006).

Fractures don't always enhance fluid transfer; some might act as flow barriers. Nelson (2001) divides NFR in 4 categories, according to what extent fractures provide porosity (i.e. oil in place) and permeability (i.e. flow capacity). In type 1 reservoirs, fractures provide most of porosity and permeability. In type 2 reservoirs, fractures provide most of permeability. In type 3 reservoirs, fractures add to permeability. In type 4 reservoirs, fractures don't add to permeability, they rather represent barriers that hinder or even prevent flow.

Over the last decades different approaches for the modelling of NFR evolved. They can roughly be categorized in three groups: (1) discrete fracture networks (DFN; Long et al., 1982), (2) dual porosity modelling (Warren & Root, 1963) and (3) single porosity modelling. DFN are especially applicable for the simulation of type 1 reservoirs, where matrix hardly contributes to production. Each fracture is modelled explicitly (line elements in 2D, disk elements in 3D) and the simulation domain is populated by fractures with properties based on statistics. The limiting factor for DFN lays in the number of fractures that can be depicted explicitly and computer power. It is also possible to incorporate matrix-fracture flow with transfer functions or to enhance DFN models to discrete fracture and matrix models (Kim & Deo, 2010). Dual porosity models are based on the assumption that the whole reservoir domain can be divided into two sub-domains: a permeability-providing fracture domain and a porosity-providing matrix domain. A transfer term determines the communication between fracture and matrix domain and there is no flow within the matrix. These models are commonly used for the simulation of type 2 reservoirs. A possible enhancement are dual porosity, dual permeability models that also incorporate flow within the matrix. Some authors introduced a trial porosity model, with two different matrix domains (e.g. Abdassah & Ershaghi, 1986). Single porosity models are not very different from classical reservoir simulators. Here, fracture and matrix properties (i.e. porosity, permeability, compressibility) are combined to provide one single value that should describe the reservoir unit accurately. Single porosity models are typically used for the simulation of type 3 reservoirs.

The most relevant feature in a dual porosity model is the flow between matrix and fracture. Mathematically it is described using a transfer term. This transfer term depends heavily on a variable called shape factor. Despite its name this parameter does not only incorporate the shape of the matrix blocks, but also is influenced by the character of the underlying physical recovery mechanism (e.g. convection or diffusion) and the flow regime (e.g. pseudo steady-state or transient) (Van Heel & Boerrigter, 2006). However, despite decade-long research it is not clear how the shape factor can be calculated. Even for the simplest geometry (rectangular cuboid matrix blocks) many different formulas have been proposed in the literature (e.g. Warren & Root, 1963; Kazemi et al., 1976; Coats, 1989; Ueda et al., 1989; Chang, 1993; Lim & Aziz, 1995).

In this thesis I use a single porosity model to estimate the shape factor for a dual-porosity cell of the same field-like size. I also simulate water alternating gas (WAG) injection and provide a model to estimate recovery factor as a function of the percentage of fractures filled.

This thesis starts with an introduction into the most important background topics of the thesis. The dual porosity model is discussed in more detail and an overview about equations for a shape factor is given. Additionally, basic information about injection is given. Subsequently, the methodology of the study is described. It starts with an overview about the geological data that have been used as a basis. Then, the properties that are necessary for simulation are described and how they were obtained for the study.

Chapter 2

Background

2.1 Dual Porosity Models

The theoretical framework for dual porosity (DP) models was laid by Barenblatt, Zheltov & Kochina (1960). These authors already recognised the necessity for two over-lapping media to accurately describe the effect of fractures. Warren & Root (1963) introduced the concept of DP into the reservoir engineering community using their famous sugar cube model (Fig. 2.1). At each point in space and time there exist two pressures and two media: matrix and fracture. Each medium has distinct properties, such as porosity, permeability and compressibility. Geometrically, matrix blocks are surrounded by up to three perpendicular sets of fractures (in x-, y- and z-direction, respectively). In the sugar cube model there are three sets of fractures, but it is also possible to model only one or two sets. In practise, matrix blocks are mostly represented as rectangular cuboids. Sometimes all three sides have the same length (making the matrix block a cube, as in the sugar cube model), but again this is no mandatory condition. For the rest of this paper, shape factors (if not mentioned otherwise) refer to rectangular cuboids. The reservoir domain can then be up scaled using the continuum approach and formulated with properties taken over a representative elementary volume, just as it is done for single continuum. It is important to note, that a computational grid cell normally includes many matrix blocks. Therefore, 'matrix block' is not a synonym for 'matrix cell'. This distinction will be highlighted in the description of the single porosity model. In the work of Warren & Root (1963) flow happens only between neighbouring fracture cells, but there is no flow between adjacent matrix blocks. The flow between matrix and fracture is then incorporated via a transfer function. Equations 2.1 - 2.3 show a simple, one-phase DP model, where the transfer function can be seen in equation 2.2.

$$\frac{\delta}{\delta x}\left(\frac{k_{f,eff}}{\mu}\frac{\delta p_f}{\delta x}\right) + \hat{q} - \tau = \phi_f c_f \frac{\delta p_f}{\delta t} \tag{2.1}$$

$$\tau = \sigma \frac{k_m}{\mu}(p_f - p_m) \tag{2.2}$$

$$\tau = \phi_m c_m \frac{\delta p_m}{\delta t} \tag{2.3}$$

The significant factor in the transfer function is the shape factor σ. Despite its name the shape factor does not incorporate only the shape of the matrix block, but also the character of the underlying physical recovery mechanism (e.g. convection or diffusion) and the flow regime (e.g. pseudo steady-state or transient) (Van Heel & Boerrigter, 2006). Initially, the DP was mainly used for the interpretation of well tests (Warren & Root, 1963; Kazemi, 1969), but soon scientists started to use the concept for reservoir simulation. Kazemi et al. (1976) were the first that programmed a simulator that is able to handle three-dimensional, three-phase multiple-well scenarios. From a theoretical point of view, at least five main recovery mechanisms are involved in the transfer of oil from the matrix blocks to the fracture: fluid-expansion, viscous forces, capillarity, gravity drainage and diffusion (Abushaikha & Gosselin, 2008). While fluid-expansion and diffusion are commonly not very significant driving forces, viscous forces and capillarity have already been accounted for in Kazemi et al. (1976).

Gravity drainage forces are caused by different densities. When the fluid saturations in matrix block and fracture are not the same, a hydraulic head will prevail. This effect occurs even when fracture and matrix pressure is the same and it may force water into the matrix blocks and oil out of them. Gravity drainage was implemented within the framework of DP by Gilman & Kazemi (1983) and Gilman (1986) by extending the transfer function and introducing a new gravity drainage shape factor. Attempts to incorporate diffusion and fluid expansion have been made (e.g. Lu et al., 2008), but due to their complexity they don't have much influence on industry reservoir simulation.

Over the last decades, many improvements and adjustments for the classical DP have been introduced. Arguably the most-known one is the dual porosity, dual permeability (DPDP) model. It was introduced by Blaskovitch et al. (1983) and assumes fluid flow also within the matrix blocks. As neither geometry nor flow regime change, a reservoir would have the same shape factor for both the DP and the DPDP model. DP models can also be extended to triple or multiple porosity models, when a third medium is thought to be necessary to capture reservoir behaviour accurately (e.g. Abdassah & Ershaghi, 1986). The multiple interacting continua (MINC) model was introduced by Pruess & Narasimhan (1985) and replaces the matrix block by a number of cells with decreasing size.

2.2 Different Equations for the Shape Factor

The history of equations for the shape factor is necessarily closely linked to the history of the dual porosity model. It is not surprising that the first equation (equation 2.4) for a shape factor was already included in Warren & Root (1963). However, there is no explanation in their paper how they have derived it.

$$\sigma_{WR} = \frac{20}{3}\left(\frac{1}{L_x} + \frac{1}{L_y} + \frac{1}{L_z}\right) \tag{2.4}$$

Kazemi et al. (1976) found a slightly different formulation for the shape factor, which was derived by using a final difference formulation (equation 2.5).

$$\sigma_K = 4(\frac{1}{L_x^2} + \frac{1}{L_y^2} + \frac{1}{L_z^2}) \tag{2.5}$$

Coats (1989) agrees with the structure of Kazemi et al., but uses a pre-factor of 8 instead of 4. Ueda et al. (1989) compared fine grid simulations with DP simulations and noted that the pre-factor of Kazemi et al. should be multiplied by 2-3. Up to that paper, all authors assumed the flow regime to be pseudo-steady-state. Chang (1993) based his derivation on a transient flow regime and therefore obtained a time-dependent shape factor. However, the asymptotic value of the shape factor (which is reached after a short time) resembles the shape factor equation of Kazemi et al., but uses a pre-factor of π^2=9.87 instead of 4. The same time-dependent result was reached independently by Liam & Aziz (1994), who used a different derivation.

A general equation describing the shape factor for any kind of geometry was presented by Kazemi, Gilman & El Sharkawy (1992) and later re-derived by Heinemann & Mittermeir (2012). Applied to a rectangular cuboid matrix block it follows that $\sigma_K = \sigma_{KGE}$.

$$\sigma_{KGE} = \frac{1}{V} \sum_{i=1}^{n} \frac{A_i}{d_i} \tag{2.6}$$

Lu et al. (2008) introduced a general transfer function that also incorporates molecular diffusion and fluid expansion and therefore goes beyond the mere shape factor concept. However, this approach is rather difficult to implement and has up to now only found relevance in the scientific community.

2.3 Water-Alternating Gas

In many miscible gas flooding projects, water is injected alternating to gas. The idea behind this is that alternating injections behind a miscible liquefied petroleum gas slug lowers the combined mobility of the fluids, prevents viscous fingering and improves volumetric sweep efficiency (Dyes, 1963). Huang & Holm (1988) define WAG as a planned alternate injection programme with water-to-gas injection rates of 0.5 to 4 volumes of water to 1 reservoir volume of gas at alternation frequencies of 0.1 to 2% PV slugs of each fluid. Over the last decades, WAG has developed to an increasingly popular enhanced oil recovery method. Christensen (2001) reviewed more than 60 fields where WAG projects have been implemented and found increased oil recovery in the range of 5 to 10% of the oil initially in place. In NFR, fractures improve the communication between gas and the oil in the rock matrix, which is one reason why gas injection is very popular in fractured reservoirs (e.g. O'Neill, 1988). Additionally, the danger of early gas breakthrough is especially high in class 2 NFR, as fractures provide a pathway for the gas.

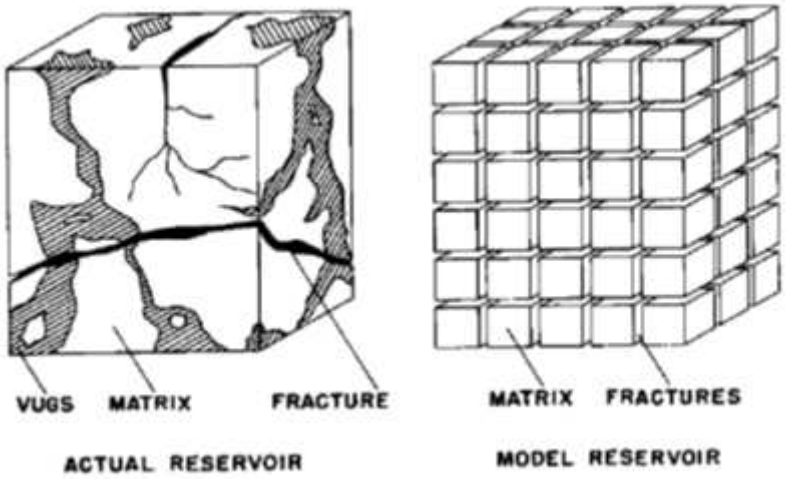

Figure 2.1: Dual Porosity Model, taken from Warren & Root (1963).

Chapter 3

Methodology

3.1 NFR Setting/Geological Model

The geological data for this thesis have been recorded near the Wiestal - Stausee, north of the Austrian village of Adnet in the federal province of Salzburg. The restricted lagoon of the Late Triassic Dachstein Limestone/Hauptdolomit Carbonate Platform found in this area is an excellent example of an outcrop analogue for fractured carbonate reservoirs (Boonchai, 2016).

The Late Triassic Dachstein Limestone/Hauptdolomit Carbonate Platform forms a widespread area in what was once the western part of the Tehtys Ocean (Haas et al., 1995). The Hauptdolomite and the Dolmia in the Northern and Southern Alps and the Western Carpathians are what is left today of the restricted inner lagoonal area/ platform interior (Bechtel et al., 2007). The sedimentary sequence can have a thickness up to 2,000 m, leading to a high potential for hydrocarbon formation (Tollmann, 1976). The study area was drowned in the Late Norian and transformed into the shallow neritic Kössen basin (Gawlick et al., 1999). From a tectonic point of view, the area belongs to the Osterhorn Block of the Lower Tirolic Nappe (Frisch & Gawlick, 2003). Fig. 3.1 provides a geological overview about the study area and its surroundings.

All geological data in this thesis originate from Boonchai (2016). Fig. 3.2 shows the whole outcrop, where the blue rectangle indicates the exact position of the collected section. Boonchai (2016) could identify a total of 7 individual layers, as can also be seen in Fig. 2. For each layer, rock type, fracture spacing and porosity were recorded. A total of 3 different rock types were found (Blindstone/Packstone, Wackestones and Grainstone).

Although the rock types differ geologically from each other significantly, no relative permeability measurements were performed and therefore no data are available. Differences that would be relevant for the purpose of Reservoir Engineering only occur in terms of matrix porosity and matrix permeability and they would change the recovery factor only slightly. For that reason only one rock type was taken into account for this study. Layer 3 as shown in Fig. 3.2 is a Blindstone/Packstone with an estimated porosity of 20%. Over a length of 4 m a total of 6 fractures were identified, resulting in a fracture spacing of 0.67 m.

Boonchai (2016) estimated average pore size for the matrix of each layer to

be in the order of 15 μm. Lucia (1983) published porosity-permeability correlations for non-vuggy carbonate rock types and different average pore sizes. These correlations were applied to the layers in the table, yielding an absolute permeability of 10 mD for the layer used in this study. Rock compressibilities were calculated based on the results obtained by Harari, Shu-Teh & Saner (1995). They were found to be 2.37e-5 1/kPa for Packstones at field unit standard conditions (14.7 psi).

For the purpose of this study it is assumed that the outcrop is representative for a NFR. The reservoir is located at a depth of 2,000 m. Taking an average geothermal gradient of 25 °C/km and a surface temperature of 15 °C, reservoir temperature equals 65 °C. This value is in line with the region's CAI of 1.0 that does not indicate a temperature of more than 80 °C. Hydrostatic pressure at this depth is 19,620 kPa at a standard water density of 1,000kg/m^3.

In the reference model, all reservoir fractures are assumed to be open fractures, i.e. they are not filled by deformational or diagenetic material. Therefore they are open for fluid flow and it is reasonable to assume the reservoir to be a type 2 reservoir. For simplicity it is assumed that all fractures are vertical. The aperture of the fractures was determined to be between 1 and 2 mm, with the majority having an aperture of about 1 mm. However, such an aperture would mean an effective fracture permeability of more than 120 D, an unrealistically high value. For that reason aperture was halved, resulting in an effective fracture permeability of 15,557 mD. This value was taken for all subsequent simulations.

3.2 Fracture and Matrix Properties

Physical properties of fractures depend mainly on their mode of origin, mechanical properties of the host rock and subsurface diagenesis (Nelson, 2001). There is some ambiguity how to get the most reliable data. While Nelson (2001) claims that data derived from well logs are not accurate and inappropriate, Aquilera (1980) holds the view that little useful data can be obtained via core analysis. Simulators, such as CMG IMEX, need a couple of fracture and matrix parameters for the simulation of a dual porosity reservoir. Table 3.1 gives an overview about the necessary input properties for CMG IMEX and how they were obtained for the reference case in this study.

Over the years, equations for fracture properties from geological observations have been developed. In this thesis, equations according to Parsons (1966) and Gilman & Kazemi (1983) were used to calculate effective fracture permeability and the equation according to Gilman & Kazemi (1983) was used to calculate fracture porosity.

CMG requires defining a reference pressure, at which input reservoir properties are valid. For all simulations conducted for this thesis, a reference pressure of 101.3 kPa (sea level standard atmospheric pressure) was taken. Hence, the values recorded in the field can directly be used. Bubble point pressure is set to be 10,000kPa, so all simulations in this study occur in the under saturated oil region. The oil in the reservoir is assumed to be Brent, with a typical oil density of 837.5 kg/m^3.

Fracture compressibility can have significant influence on a NFR. Aguilera noted the influence of this property on oil recovery in stress-sensitive fields

Property	Value	Determination
Matrix Porosity [%]	20	measured in the field
Matrix Permeability [mD]	10	Lucia, 1983
Matrix Compressibility [1/kPa]	2.37e-5	Harari, Shu-Teh & Saner, 1995
Fracture Spacing [m]	0.67	measured in the field
Fracture Aperture [mm]	1	measured in the field
Effective Fracture Permeability [D]	4.5	Parsons, 1966; Gilman & Kazemi, 1983
Fracture Porosity [-]	0.001	Gilman & Kazemi, 1983
Fracture Compressibility [1/kPa]	1.92e-5	Jones, 1976
Reservoir Pressure [kPa]	19,620	hydrostatic pressure
Reservoir Temperature [°C]	65	geothermal gradient of 25°C/km
Bubble Point Pressure [kPa]	10,000	50% of reservoir pressure
Oil Density [kg/m^3]	837.3	Brent specifications
Relative Gas Density [-]	0.65	estimation
Reservoir Wettability	oil-wet	Treiber & Owens, 1976
Relative Permeability	Stone II	default model
Relative Permeability Parameter	TBA	TBA

Table 3.1: Reference Case Properties.

(Aguilera, 2006) as well as on gas-in-place calculations (Aguilera, 2008). Natural fractures initially opened because of stresses in the sub-surface. When reservoir pressure decreases because of depletion, these stresses also decrease, which may lead to the closure of fractures. The permeability of a fracture is proportional to the square of the fracture aperture. As fractures represent most of the permeability of the reservoir, fracture compressibility can have a significant influence on ultimate recovery. The value used in this thesis was calculated using the equation published by Jones (1976). However, CMG does only allow one input value for rock compressibility in the single porosity model, which is the reason why for the single porosity model only the rock compressibility of the matrix is used. As both values are pretty close, there should not be much error. For the dual porosity model, both the matrix and the fracture compressibility were used.

Treiber & Owens (1976) noted after the investigation of more than 55 NFR that carbonate reservoirs tend to be oil-wet, while sandstone reservoirs tend to be equally oil- and water-wet. This result was also confirmed by other authors (e.g. Bennion et al., 2002; Hollis et al., 2010). For that reason, it is defined that for the reference case in this study the carbonate layer is oil-wet.

Three-phase relative permeabilities are calculated using the Stone II model (Stone, 1973) modified by Aziz & Settari (1979). This model is widely used and an industry standard. When simulating the single-porosity model it is necessary to create two rock-fluid-types: one for the matrix and one for the fracture. The focus of this thesis does not lay on relative-permeability relationships. For that reason the default values of CMG were used to characterize matrix rock-fluid-relationship. They can be found in table 3.2. To describe rock-fluid interaction a simple model with linear relative permeabilities and no connate phase satu-

$S_w[-]$	$k_{rw}[-]$		$k_{rw}[-]$	
	Oil Wet	Water Wet	Oil Wet	Water Wet
0.2	0	0	0.3	0.8
0.225	0.003125	0.001172	0.263672	0.703125
0.25	0.0125	0.004686	0.229688	0.6125
0.275	0.028125	0.010547	0.198047	0.528125
0.3	0.05	0.01875	0.16875	0.45
0.325	0.078125	0.029297	0.141797	0.378125
0.35	0.1125	0.042188	0.117187	0.3125
0.375	0.153125	0.057422	0.094922	0.253125
0.4	0.2	0.075	0.075	0.2
0.425	0.253125	0.094922	0.057422	0.153125
0.45	0.3125	0.117187	0.042188	0.1125
0.475	0.378125	0.141797	0.029297	0.078125
0.5	0.45	0.16875	0.01875	0.05
0.525	0.528125	0.198047	0.010547	0.028125
0.55	0.6125	0.229688	0.004688	0.0125
0.575	0.703125	0.263672	0.001172	0.003125
0.6	0.8	0.3	0	0

Table 3.2: Relative Permeability Curves Matrix.

rations is used.

To account for capillary effects, a capillary pressure curve based on the Brooks-Corey model was used. Exact values for the matrix can be found in table 4. For the fracture all capillary pressure values were set to zero, with the exception being a water saturation of 0, where a capillary pressure of 16.67 kPa was used (as inspired by Gilman & Kazemi, 1973). As there are no data available for the rock, the used curve is symmetric (i.e the area between the positive part of the curve and the x axis equals the area between the negative part of the curve and the x axis) and used for the oil wet rock. For the water wet rock, such a curve is not realistic at all, as capillary pressure is usually not negative. To account for this, negative values are set to zero, while the positive values are kept the same. No capillary curve for liquid-gas is taken into account.

3.3 Single Porosity Model

The single porosity model is a cube comprised of 34 cells on each side, resulting in a total of 39,304 cells. There are two different types of cells (matrix cells and fracture cells) that build a pattern equivalent to the sugar cube model. The top layer of each side consists of fracture cells with a height of 0.01 m, and is then followed by 10 matrix cells (each of the matrix cells has a height of 0.067 m, resulting in a total height of 0.67 m). Then the same cycle (1 layer of fracture cells followed by 10 layers of matrix cells) starts again. The bottom layer of each side consists of fracture cells again. Altogether there are 27,000 matrix cells and 12,304 fracture cells. Fig. 3.3 shows the single porosity model.

All fracture cells are set to an initial water saturation of 100% and all matrix cells have an initial water saturation of 20%. The imbibition process is simulated not by injecting wells, but by the usage of pore volume multipliers

$S_w[-]$	$P_c[kPa]$
0.2	16.67
0.225	11.67
0.25	8.33
0.275	5.95
0.3	4.17
0.325	2.78
0.35	1.67
0.375	0.76
0.4	0
0.425	-0.76
0.45	-1.67
0.475	-2.78
0.5	-4.17
0.525	-5.95
0.55	-8.33
0.575	-11.67
0.6	-16.67

Table 3.3: Capillary Pressure Matrix.

(keyword VOLMOD in CMG). Pore volumes are then calculated by multiplying porosity (which itself is a function of pore pressure and compressibility) with the multiplier. This function can be used to model reservoir boundaries using a multiplier below one (CMG, 2013), but must necessarily be way higher for this study. However, initially it is not clear what exact value should be used. For that reason a sensitivity analysis was performed to estimate the influence of the volume multiplier on ultimate recovery. For this sensitivity analysis only the injection of water and viscous driving forces were considered.

As mentioned above, WAG processes play an important role in NFR. For this thesis a simplified WAG process was performed. At first water is injected (i.e. water saturation in the fracture cells equals 100%). Oil recovery over time is then recorded. Once the marginal recovery of water injections flattens out, gas is injected (i.e. a new simulation is performed where gas saturation in the fracture cells is set to 100% and saturation in the matrix cells are set to the values of the initial simulation's last time step). The simplified WAG process is performed both for the oil wet and the water wet rock. There is a small error in WAG simulations, as CMG sets bubble point pressures to reservoir pressure in the presence of gas. For that reason, for some time steps, oil volume expands as gas is dissolved leading to a decreased in recovery factor. As this cannot occur in reality, these values were corrected.

Due to the complexity of some of the input files, they were not written by hand, but rather generated using Python code. It was also not possible to use CMG output files directly as input files for subsequent CMG simulations (e.g. for the performance of WAG injections). For that reason Python was also used as gluing software.

3.4 Dual Porosity Model

CMG supports the creation of dual porosity models. The geometric representation of such models is very equal to single porosity models with the only difference being that each cell now contains two continua. The same dimensions as for the single porosity model have been taken; however, the whole model consists of only one cell, as can be seen in Fig. 3.4. Properties are taken from table 2. It is only possible to specify one rock type; therefore the capillary pressure curve for matrix was taken for the model. Although the same volume multipliers were set as for the single porosity model, this did not lead to any fluid movements. Therefore, the only driving force for DP simulations is capillarity. It is also important to highlight, that CMG does not support the simulation of gravity drainage in the DP model, i.e. fluid movement due to density differences between oil and water and different saturations in matrix and fracture.

3.5 Finding Shape Factors

In the literature there is a lot inconsistency about how to calculate shape factors(e.g. Warren & Root, 1963; Kazemi et al., 1976; Coats, 1989; Ueda et al., 1989; Chang, 1993; Lim & Aziz, 1995). The two most commonly used equations originate from Warren & Root (1963) and Kazemi et al. (1973). Those two formulas are implemented in CMG and one of them can be chosen for calculations. The idea is to fit the shape factor of the DP model (via changes in fracture spacing) in such a way that both single porosity and dual porosity model obtain the same results in terms of recovery factor. However, this endeavour can only be an approximation. The main reason for this are different driving mechanisms. For the single porosity model, flow is driven by viscous forces as well as by capillary forces. For the dual porosity model the only driving force is capillarity.

3.6 Fracture Filling

Grid cells used in the simulation of full-field reservoirs are normally in the size of 25 to 50 m (while representing the true layer thickness). Running a simulation with a model that has more fracture sets than the single porosity model described above has no influence on recovery factor. This fact is shown when comparing recovery factor for a model with a cell size of 111x111x34 cells (i.e. for 10 matrix blocks in horizontal direction) to the reference model. Recovery factor over time is equal to the reference single porosity model (with 3 matrix blocks in each dimension).

Not every fracture that is recorded by geologists is always fully open. It is realistic that a certain percentage of fractures is filled, as mineral deposits in fractures are wide spread. They range from isolated crystals that only decrease fracture aperture to massive cements that totally fill the fracture (Laubach, 2003). It is therefore an interesting question what happens to recovery factor if a certain percentage of fractures in the single porosity model are filled. To estimate this effect, a modification is applied on the single porosity model. There are n fractures in x as well as in y direction, for a total of n^2 fractures in the horizontal plane. A certain percentage of these fractures is then considered to be inactive, i.e. the corresponding cells have the properties of matrix cells,

although the size of the cells does not change. Active and inactive fractures are assigned randomly. Fig. 3.5 depicts this principle.

Simulations with different percentages of fractures filled are run for a model with a cell size of 111x111x34 cells (i.e. for 10 matrix blocks in horizontal direction). This size provides a reasonable balance between accuracy and computing time.

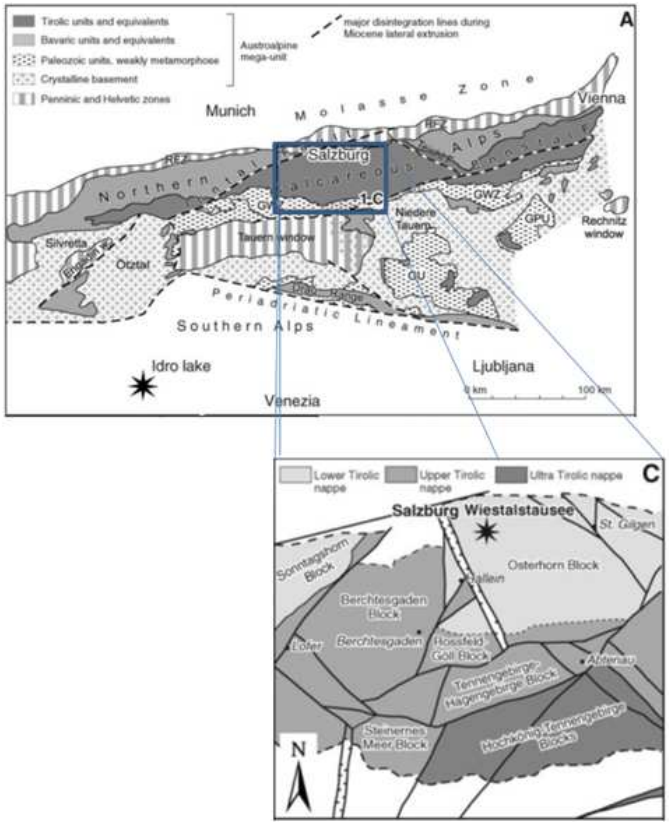

Figure 3.1: Location of the Study Area. a) shows the tectonic map of Western Austria and the study area. b) depicts block configuration of Northern Calcareous Alps. Modified after Bechtel et al., 2007.

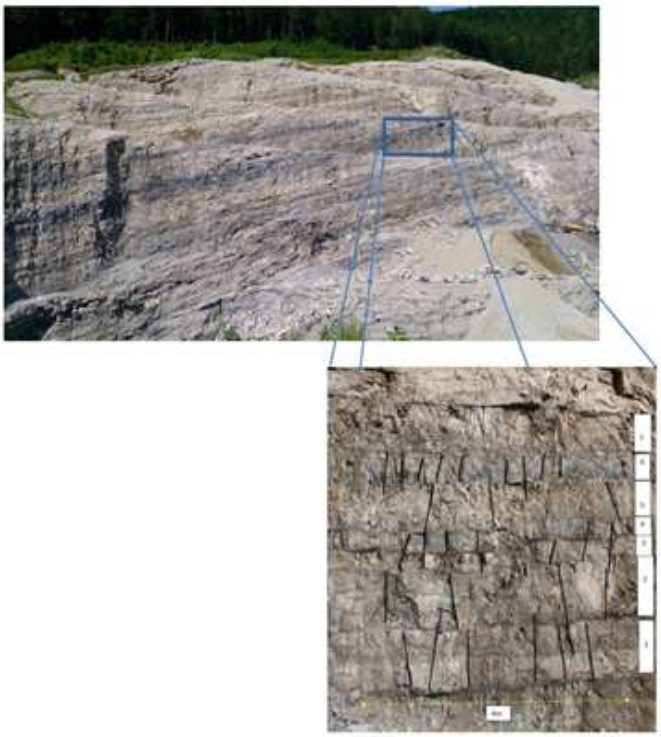

Figure 3.2: Geological Outcrop. 2a) shows the outcrop. 2b) depicts individual layers that have been identified by Boonchai (2016) - natural fractures are highlighted by black lines.

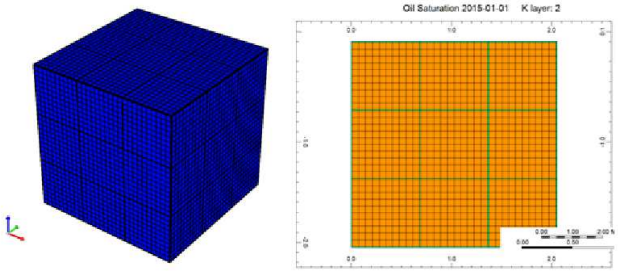

Figure 3.3: Single Porosity Model. a) shows a 3D image of the model. As the outermost cells are all fractures they have homogeneous properties. The size of the cells gives nevertheless an idea of the principle. b) shows the cross section of the model for a layer within the model. Here the difference between the two domains is easy to see. Matrix cells are indicated by yellow, while fracture cells are indicated by green.

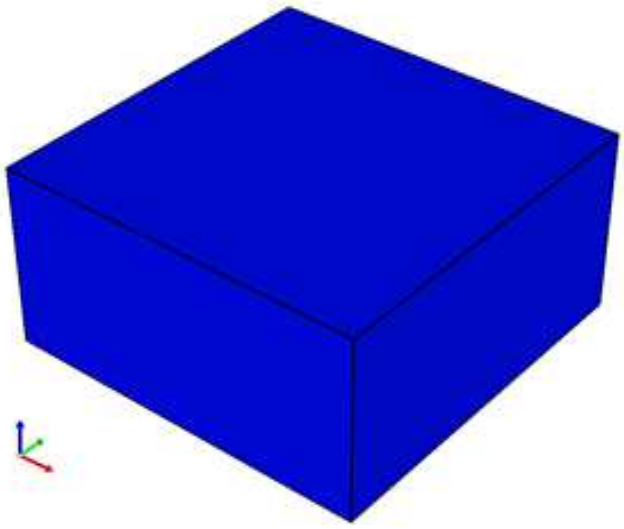

Figure 3.4: Dual Porosity Model. The whole model consists of only one cell. All sides have the same length making the model a cube, although this not shown accurately by CMG.

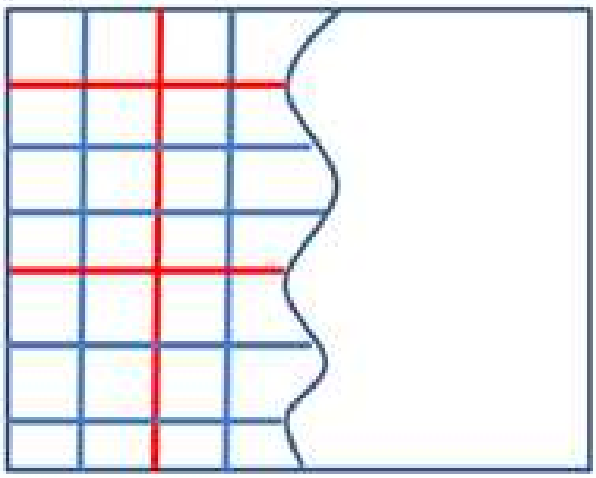

Figure 3.5: Principle of Fracture Filling. As in simulations above, fractures form a chessboard pattern. Some of them are active fractures (blue), while others are inactive (red). This property is assigned randomly.

Chapter 4

Results

All charts in this chapter depict the development of recovery (RF) factor over time. The recovery factor is used during the thesis as follows.

$$RF = (1 - \frac{oil_{remaining}@SC}{STOOIP}) \times 100 \tag{4.1}$$

As the pressure is de facto constant for all grid blocks during the simulations (a maximum deviation of less than 20 kPa at an average pressure of 20,000 kPa), the same result is obtained when oil at reservoir conditions is used instead of oil at standard conditions. The data were compiled using Python, which gives more freedom in terms of data manipulation than the usage of the graph application that is shipped with CMG.

4.1 Sensitivity Analysis Volume Multiplier

Six different values for the volume multiplier were used to estimate its influence on the RF. All simulations start with January 1, 2015 and values are recorded every 5 days till December 27, 2015. Figure 4.1 shows the obtained results.

Recovery curves show significant deviation between different volume multipliers, both in the curve behaviour within the first three months and in the reached plateau value (ultimate recovery after one year). A multiplier of e+4 does not make much sense. Due to the significant difference between matrix and fracture porosity, this value is not high enough to simulate the desired process. The behaviour in the first months of curves obtained by volume multipliers between e+5 and e+8 is very similar. However, the plateau value differs, as the value obtained by a multiplier of e+5 is significantly below the values obtained by multipliers of e+6 to e+8 (about 42%). A multiplier of e+9 leads to a shape that once again is very different from former results. Here and at higher multipliers, numerical errors start to occur that lead to unnatural results. This is not very surprising, as CMG's manual recommends using a multiplier less than e+4 (CMG, 2013). When the same process is repeated for the water wet rock, results are very similar, although plateau recovery factor reaches about 47% after the same time period. For all subsequent simulations in this thesis, a volume multiplier of e+7 is used, as this value obviously makes the most sense.

4.2 Water Injection Only

When water is injected into an oil bearing NFR, displacement is starting upwards, as water enters from the bottom due to its higher density compared to oil. This phenomenon can be seen in Fig. 4.2.

The results for recovery factor over time can be seen in Fig. 4.3. There is significant deviation between different recovery mechanisms and rock types. The recovery only based on the viscous driving force happens much slower. Here, recovery for the water wet rock is much higher than for the oil wet rock as one would expect. On the other hand, a combined recovery mechanism (i.e. capillarity and viscous forces) leads to a sudden increase in recovery factor, but after this initial effect there is not much rise. It seems that some equilibrium is reached after one month in the simulations used for this thesis. Strangely enough, the oil wet rock has a recovery that is almost twice the recovery of the water wet rock. This is due to the capillary pressure curve that is used for the fracture. If the fractures' capillary pressure curve for the oil wet rock is set to zero, recovery for the oil wet rock equals roughly recovery for the water wet rock. Attempts to simulate only capillary as driving force in the single porosity model (i.e. setting the volume multiplier to zero) lead to abnormal program termination, as CMG cannot converge.

4.3 Water Alternating Gas Simulations

As seen in the previous section, recovery flattens after a short time. The plateau is reached very quickly if both driving forces are considered and it is reached a bit slower if only viscous forces are taken into account. This is a sub-optimal outcome in both scenarios. The injection of gas leads to a downwards replacement effect, where gas is coming from top (due to its lower density compared to the two liquids). This can be seen in Fig. 4.4.

Fig. 4.5 and Fig. 4.6 show the results of the WAG simulations – both if only viscous forces are considered and if viscous forces are considered in addition to capillary forces. It is remarkable that in all four cases the same ultimate recovery factor is reached. Neither wettability nor driving forces do matter – ultimate recovery factor after one year is always slightly below 70%. While recovery factors vary significantly if only water in injected, this is balanced by the start of gas injection. In all cases gas replaces water coming from the top and leading to a huge surge within a short time (in the order of 10 days). After the surge is completed, recovery factor rises slowly. This is even the case if both capillary and viscous driving forces are considered – contrary to what is seen if only water is injected.

In reality, WAG injection does not end after one cycle, but rather is repeated over and over again. As one can see from Fig. 4.6 and 4.7, recovery in the gas injection part is increasing only slowly after the initial surge. However, gas is generally more expansive than water, and therefore it makes sense to ask, what happens, if one would inject water sometimes after the gas injection. The result is seen in figure 4.8. In the simulation, additional water injection has no effect. Recovery factor keeps constant.

4.4 Dual Porosity Simulations

The first main aim of this thesis is to find a correction factor that modifies the shape factor of the DP model in such a way that dual porosity and single porosity model obtain the same result. However, the shape factor is calculated internally in CMG and it is therefore not possible to modify it directly. As mentioned in a previous chapter, the shape factor using the equation of Gilman & Kazemi (1973) only depends on the distances between the individual fractures. So the idea is to modify the fracture distances und record the difference between the new dual porosity curve and the single porosity curve. The minimum deviation for the first 30 days gives than the 'right' fracture distance, which enables to calculate the correction factor. During the process all other parameters are kept constant. There is a whole array of ways how the difference between two sets of values can be calculated. For this thesis the simplest one is taken: the sum of the absolute value of the differences between the two curves.

$$difference = \sum_{i=1}^{n} |x_i - y_i| \tag{4.2}$$

Fig. 4.9 shows the comparison of single porosity and dual porosity model if this process is applied to the oil wet rock. A 'right' fracture distance of 0.49 m was found resulting in a difference of 5.48 m. This is equivalent to a correction factor of 1.8696, meaning that the corrected equation for the shape factor can be written as following. If the corrected shape factor is used there is hardly any difference between recovery curves calculated by the single and the dual porosity model.

$$\sigma_K = 7.4785(\frac{1}{L_x^2} + \frac{1}{L_y^2} + \frac{1}{L_z^2}) \tag{4.3}$$

Results for the water wet rock can be seen in Fig. 4.10. This time, results are significantly different. As mentioned above, there are two visible recovery mechanisms in the single porosity model. This is not the case for the dual porosity model, where only capillarity acts as recovery mechanism (although volume multiplier was set to the same value as in the single porosity model). For that reason, recovery factor after six months in significantly different. The change of fracture distances does not have any meaningful effect on ultimate recovery and there is always a significant deviation no matter what is set as fracture distance. Nevertheless, it is at least possible to minimize the deviation between the two curves. By doing so, it turns out that the 'right' fracture distance is 0.26 m, resulting in a high difference of 69.83. This is equivalent to a correction factor of 6.6405, meaning that the corrected equation for the shape factor can be written as following. It is clear that this result needs to be taken with a grain of salt.

$$\sigma_K = 26.562(\frac{1}{L_x^2} + \frac{1}{L_y^2} + \frac{1}{L_z^2}) \tag{4.4}$$

4.5 Fracture Filling

Fig. 4.11 shows the oil saturation after 5 days if some of the fractures are filled. It is clearly visible from the oil saturation pattern which fractures are active and which ones are not. Fig. 4.12 depicts the effect of fracture filling on recovery over time. Despite the fact that for the yellow line 90% of all vertical fractures are filled, there is no significant deviation in recovery compared to the case when all vertical fractures are open. Significant losses in recovery only occur when one of the (middle) horizontal fractures is filled, as depicted by the black line. The recovery factor gap that widens at the beginning of the simulation closes at a later stage. This fact is also confirmed by longer running simulations whose results are not depicted here. If enough time passes by, recovery factor is almost the same. It seems that the number of open fractures just describes the rate of oil recovery and not the recovery that is achieved at the end.

Something similar occurs, if also capillarity is taken into account, as can be seen in Fig. 4.12. The yellow line indicates recovery if all fractures are open 100%. If a certain percentage of them is filled, recovery decreases, as one would expect. However, the effect is even less significant than to the situation when only viscous forces are considered. This time, even the filling of one of the horizontal fractures has no visible impact.

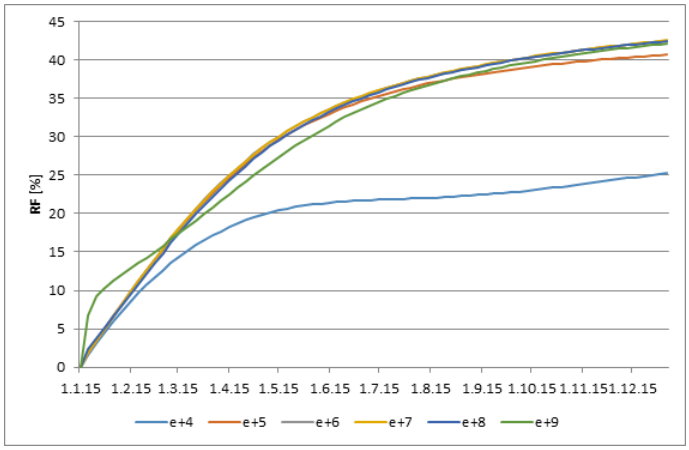

Figure 4.1: Results of VOLMOD Sensitivity Analysis. The different curves refer to different volume multipliers.

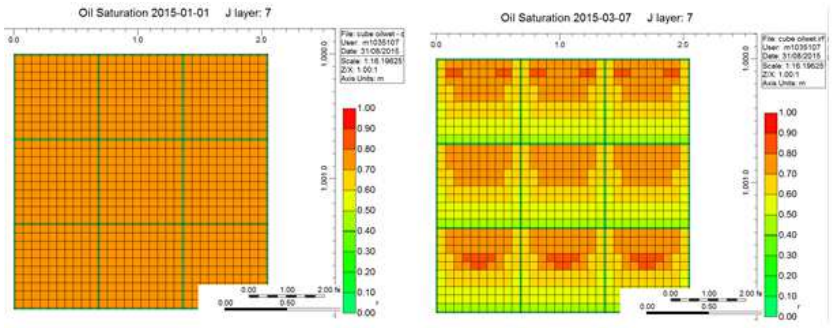

Figure 4.2: Water Injection. Due to its high density water is coming from the bottom. The highest oil concentrations can be found near the top of the block.

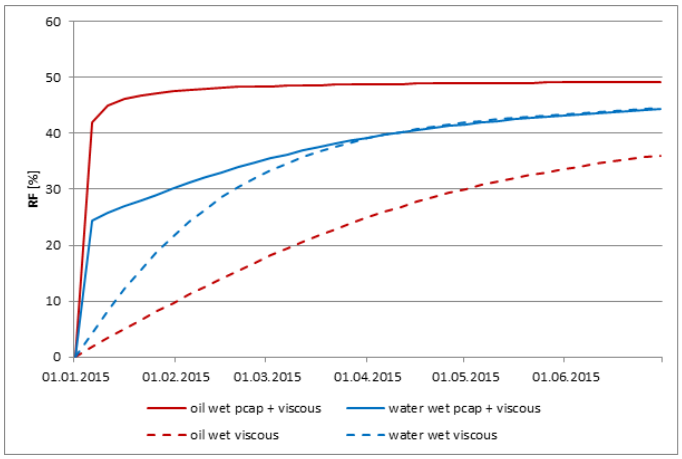

Figure 4.3: Results for Water Injection Only. Significant differences can be seen between the individual curves. Wettability as well as driving mechanisms have influence on both shape and ultimate recovery after six months.

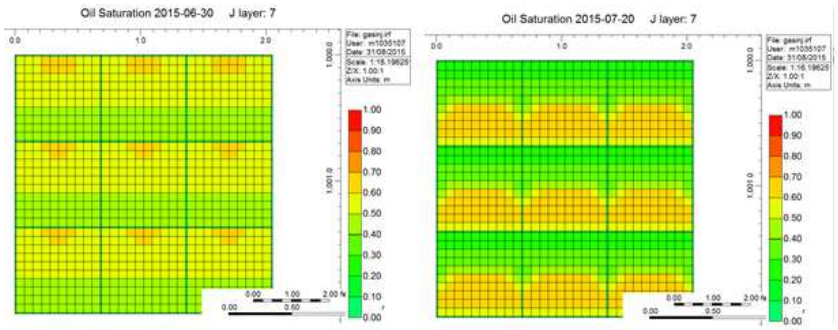

Figure 4.4: Displacement Induced by Gas Injection. Due to its low gravity gas is coming from the top of the block. The highest oil concentrations after some time can be found near the bottom of the block.

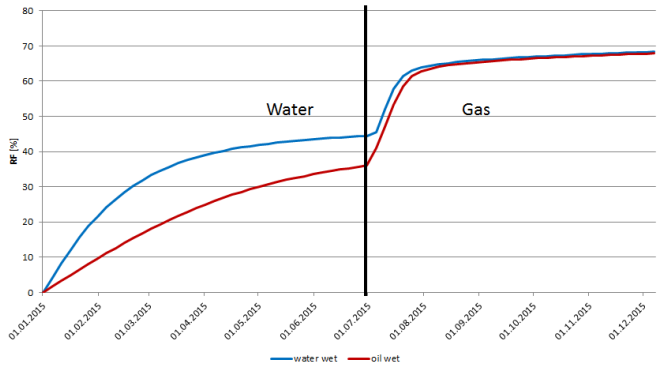

Figure 4.5: WAG Injection Only Considering Viscous Driving Forces.

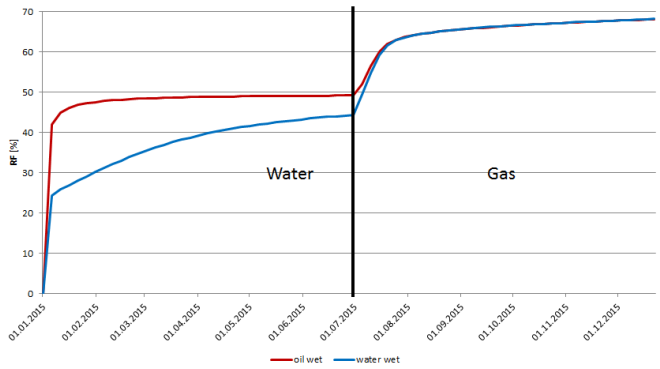

Figure 4.6: WAG Injection Considering Both Viscous and Capillary Driving Forces.

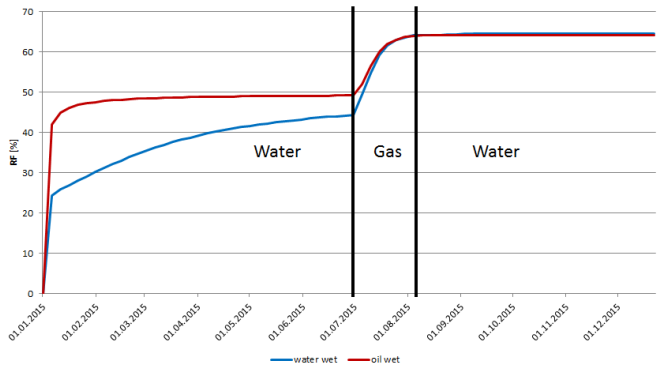

Figure 4.7: WAG Injection with Additional Water Injection. There is no gain in terms of recovery factor visible.

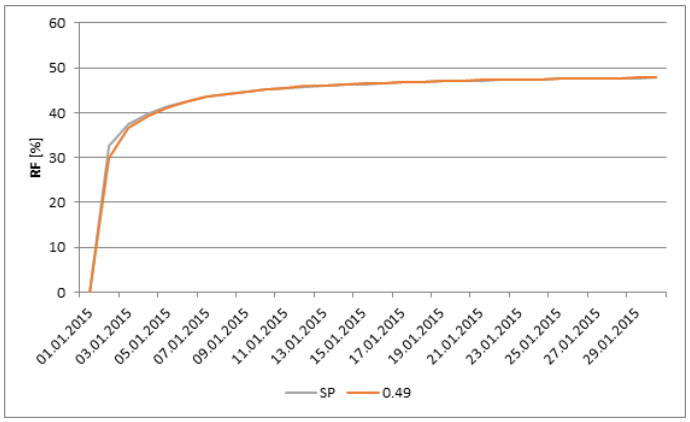

Figure 4.8: Comparison between Single Porosity and Corrected Dual Porosity Model Oil Wet Rock. The orange line refers to a fracture distance of 0.49m in all three directions.

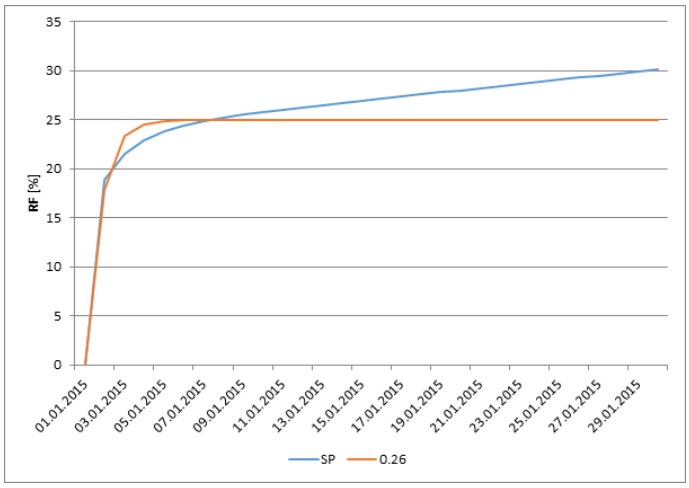

Figure 4.9: Comparison between Single Porosity and Corrected Dual Porosity Model Water Wet Rock. No matching is possible as equilibrium recovery factors deviate significantly.

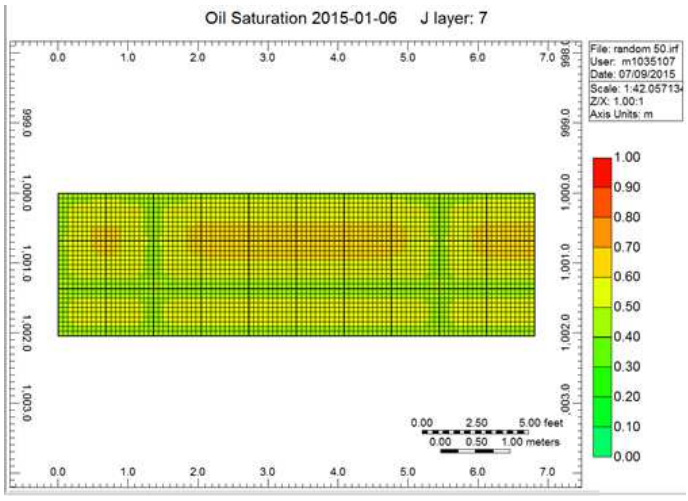

Figure 4.10: Patterns in Oil Saturation. Which fractures are filled can be easily seen by looking at the oil saturation patterns.

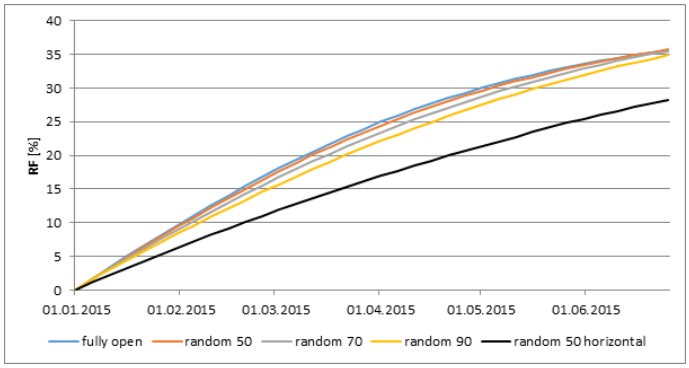

Figure 4.11: Recovery Factor if Some Fractures are Filled – Only Viscous Forces. Only the filling of a horizontal fracture makes a significant difference.

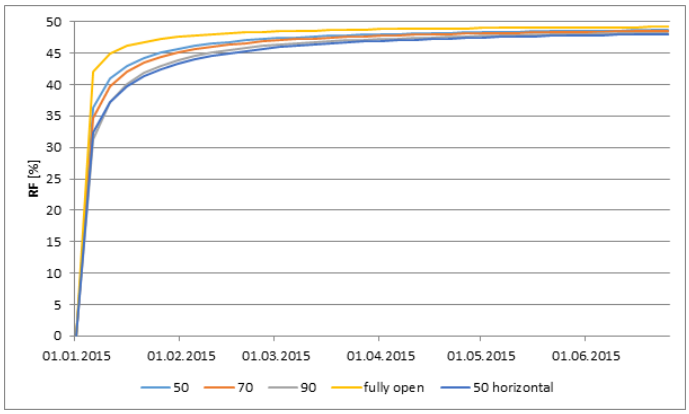

Figure 4.12: Recovery Factor if Some Fractures are Filled – Viscous and Capillary Forces. Hardly any difference in recovery is visible.

Chapter 5

Discussion and Conclusion

Within this thesis a couple of aspects regarding shape factor estimation and WAG injection in NFR are investigated.

Geological data from Salzburg are used for this thesis. All other necessary input parameters are estimated via correlation and literature. Subsequently, the single porosity and the dual porosity model are presented in detail. The experiments that are necessary for the aims of the thesis are discussed in detail. Shape factor is estimated by comparing results for a single and a dual porosity model. A WAG cycle is simulated by the subsequent simulation of fractures that are full of water and gas, respectively.

Additionally, an algorithm is described that estimates ultimate recovery as a function of the percentage of fractures filled.

For the model used in this thesis a volume multiplier of e+7 makes most sense. Multipliers that are too low cannot simulate the desired process, while multipliers that are too high lead to numerical errors.

Recovery in NFR is very much a function of the effects that are taken into account. Flow driven by capillarity leads to quick recovery, but once equilibrium is reached there is no more recovery. On the other hand, viscous fluid displacement starts slowly, but keeps adding to recovery even after one year (although at a very slow rate). Similar effects were observed by Ramirez et al. (2009). In any case, the exact formulation of the capillary pressure function is of uttermost importance.

Injecting gas after water leads to a surge in recovery (mainly caused by viscous forces). After this initial period, oil recovery increases only slowly. There is no change in ultimate recovery factor of oil wet rock versus water wet rock. A repetition of the cycle (i.e. an injection of water after the injection of gas) does not add to recovery. A comparison between single and dual porosity model works well for the oil wet rock. A correction factor of 1.87 applied to the equation of Kazemi et al. (1987) leads to a very good accordance. For the water wet rock, matching is more difficult, as the two driving mechanisms of the single porosity model are not depicted in the dual porosity model. A correction factor of 6.65 minimizes the error.

Size of the single porosity model does not have influence on recovery factor, as long as the underlying basic geometry is maintained. Fracture filling does not have a strong impact on ultimate recovery. If only viscous forces are considered, there is a certain affect (which is enhanced if one horizontal fracture is closed

additionally). If capillary forces are also taken into account, there is hardly any difference if a certain percentage of fractures are filled. The reason for this might be the fact that (active) fractures are still very close to each other. Therefore, the closure of some of them does not have an overwhelming effect.

Although the results presented in this thesis allow important insights, it may be beneficial to use real data. This is especially relevant for capillary pressure curves, where the usage of measured curves (different for oil wet and water wet rocks) will enhance the information value significantly. Another possible enhancement is the usage of liquid/gas relative permeability curves.

Appendix A

References

Abdassah, D., & I. Ershaghi. 1986. Triple-Porosity Systems for Representing Naturally Fractured Reservoirs. Society of Petroleum Engineers. SPE Formation Evaluation. Volume 1. Issue 2. Pages 113 – 127.

Abushaikha, A. S. & O. R. Gosselin. 2008. Matrix-Fracture Transfer Function in Dual-Media Flow Simulation: Review, Comparison and Validation. SPE-113890-MS. Europec/EAGE Conference and Exhibition. 9-12 June 2008. Rome, Italy.

Aguilera, R. 1980. Naturally Fractured Reservoirs. First Edition. PennWell Books. Tulsa, Oklahoma.

Aguilera, R. 2006. Effect of Fracture Compressibility on Oil Recovery from Stress-Sensitive Naturally Fractured Reservoirs. Journal of Canadian Petroleum Technology. Volume 45. Issue 12. Pages 49 - 59.

Aguilera, R. 2008. Effect of Fracture Compressibility on Gas-in-Place Calculations of Stress-Sensitive Naturally Fractured Reservoirs. SPE Reservoir Evaluation & Engineering. Volume 11. Issue 3. Pages 307 – 310.

Aziz, K. & A. Settari. 1979. Petroleum Reservoir Simulation. Applied Science Publishers. London, UK.

Barenblatt, G. I., I.P. Zheltov & I.N Kochina. 1960. Basic Concepts in the Theory of Seepage of Homogeneous Liquids in Fissured Rocks [Strata]. Journal of Applied Mathematics and Mechanics. Volume 24. Issue 5. Pages 1286 – 1303.

Bechtel, A., H.-J. Gawlick, R. Gratzer, M. Tomaselli & W. Püttmann. 2007. Molecular Indicators of Palaeosalinity and Depositional Environment of Small Scale Basins within Carbonate Platforms: The Late Triassic Hauptdolomite Wiestalstausee Section near Hallein (Northern Calcareous Alps, Austria). Organic Geochemistry. Volume 38. Issue 1. Pages 92-111.

Blaskovich, F. T., G. M. Cain, F. Sonier, D. Waldren & S. J. Webb. 1983. A Multicomponent Isothermal System for Efficient Reservoir Simulation. SPE-11480-MS. Middle East Oil Technical Conference and Exhibition. 14-17 March. Manama, Bahrain.

Boonchai, N. 2016. Title yet not defined. Master Thesis. Leoben, Austria.

Bennion, D., F. Thomas, B. Schulmeister & T. Ma. 2002. A Correlation of Water and Gas-Oil Relative Permeability Properties for Various Western Canadian Sandstone and Carbonate Oil Producing Formations. Paper 2002-066. In Proceedings Canadian International Petroleum Conference, June 11 –

13. Calgary, Canada.

Chang, M. 1993. Deriving the Shape Factor of a Fractured Rock Matrix. Technical Report NIPER-696 (DE93000170). NIPER, Bartlesville, Oklahoma.

Christensen, J. R., E. H. Stenby & A. Skauge. 2001. Review of WAG Field Experience. SPE Reservoir Evaluation & Engineering. Volume 4. Issue 2. Pages 97 -106.

CMG. 2013. IMEX User Guide. Version 2013. Calgary, Canada.

Coats, K. H. 1989. Implicit Compositional Simulation of Single-Porosity and Dual-Porosity Reservoirs. SPE-18427-MS. SPE Symposium on Reservoir Simulation. 6-8 February. Houston, Texas.

Dyes, A. B. 1963. Method for Increasing Recovery of Oil. US Patent No. 3,096,821. July 9.

Energy Information Administration. 2015. Annual Energy Outlook 2015 with Projections to 2040. DOE/EIA-0383 (2015). EIA. Washington, DC.

Frisch, W. & H.-J. Gawlick. The Nappe Structure of the Central Northern Calcareous Alps and its Disintegration during Miocene Tectonic Extrusion—a Contribution to Understanding the Orogenic Evolution of the Eastern Alps. 2003. International Journal of Earth Sciences (Geologische Rundschau). Volume 92. Issue 5. Pages 712 – 727.

Gawlick, H.-J., W. Frisch, A. Vecsei, T. Steiger & F. Böhm. 1999. The Change from Rifting to Thrusting in the Northern Calcareous Alps as Recorded in Jurassic Sediments. Geologische Rundschau. Volume 87. Issue 4. Pages 644 – 657.

Harari, Z., W. Shu-Teh & S. Salih. 1995. Pore-Compressibility Study of Arabian Carbonate Reservoir Rocks. SPE Formation Evaluation. Volume 10. Issue 4. Pages 207 – 214.

Haas, J., S. Kovacs, L. Krystyn & R. Lein. 1995. Significance of Late Permian – Triassic Facies Zones in Terrane Reconstructions in the Alpine – North Pannonian Domain. Tectonophysics. Volume 242. Pages 19 – 40.

Heinemann, Z. E. & G. M. Mittermeir. 2012. Derivation of the Kazemi – Gilman - Elsharkawy Generalized Dual Porosity Shape Factor. Transport in Porous Media. Volume 91. Issue 1. Pages 123 -132.

Hollis, C., V. Vahrenkamp, S. Tull, A. Mookerjee, C. Taberner & Y. Huang. 2010. Pore System Characterisation in Heterogeneous Carbonates: An Alternative Approach to Widely-Used Rock-Typing Methodologies. Marine and Petroleum Geology. Volume 27. Issue 4. Pages 772 – 793.

Huang, E. T. S. & L. W. Holm. 1988. Effect of WAG Injection and Rock Wettability on Oil Recovery During CO2 Flooding. SPE Reservoir Engineering. Volume 3. Issue 1. Pages 119 -129.

Kazemi, H. 1969. Pressure Transient Analysis of Naturally Fractured Reservoirs with Uniform Fracture Distribution. Society of Petroleum Engineers Journal. Volume 9. Issue 4. Pages 461 – 462.

Kazemi, H., L. S. Merrill, K. L.Porterfield & P. R. Zeman. 1976. Numerical Simulation of Water-Oil Flow in Naturally Fractured Reservoirs. Society of Petroleum Engineers Journal. Volume 16. Issue 6. Pages 317 – 326.

Kazemi, H., J. R. Gilman & A. M. Elsharkawy. 1992. Analytical and Numerical Solution of Oil Recovery From Fractured Reservoirs With Empirical Transfer Functions. SPE Reservoir Engineering. Volume 7. Issue 2. Pages 219 – 227.

Kim, J. G. & M. D. Deo. 2000. Finite Element, Discrete-Fracture Model for Multiphase Flow in Porous Media. AIChE Journal. Volume 46. Issue 6. Pages 1120 – 1130.

Laubach, S.E. 2003. Practical Approaches to Identifying Sealed and Open Fractures. AAPG Bulletin. Volume 87. Issue 4. Pages 561 – 579.

Long, J., J. Remer, C. Wilson & P. Witherspoon. 1982. Porous Media Equivalents for Networks of Discontinuous Fractures. Water Resources Research. Volume 18. Issue 3. Pages 645 – 658.

Lim, K. T. & K. Aziz. 1995. Matrix-Fracture Transfer Shape Factors for Dual-Porosity Simulators. Journal of Petroleum Science and Engineering. Volume 13. Issues 3 - 4. Pages 169 – 178.

Lucia, F. J. 1983. Petrophysical Parameters Estimated From Visual Descriptions of Carbonate Rocks: A Field Classification of Carbonate Pore Space. Journal of Petroleum Technology. Volume 35. Issue 3. Pages 629 – 637.

Narr, W., D. S. Schechter & L. B. Thompson. 2006. Naturally Fractured Reservoir Characterization. Society of Petroleum Engineers.

Nelson, R. A. 2001. Geological Analysis of Naturally Fractured Reservoirs. Second Edition. Gulf Professional Publishing.

O' Neill, N. 1988. Fahud Field Review: A Switch From Water to Gas Injection. Journal of Petroleum Technology. Volume 40. Issue 5. Pages 609 – 618.

Parsons, R. W. 1966). Permeability of Idealized Fractured Rock. Society of Petroleum Engineers Journal. Volume 6. Issue 2. Pages 126 – 136.

Pruess, K. & T. N. Narasimhan. 1985. A Practical Method for Modelling Fluid and Heat Flow in Fractured Porous Media. Society of Petroleum Engineers Journal. Volume 25. Issue 1. Pages 14 – 26.

Ramirez, B., H. Kazemi, M. Al-kobaisi, E. Ozkan, S. & Atan. 2009. A Critical Review for Proper Use of Water/Oil/Gas Transfer Functions in Dual-Porosity Naturally Fractured Reservoirs: Part I. SPE Reservoir Evaluation & Engineering. Volume 12. Issue 2. Pages 200 – 210.

Stone, H. L. 1973. Estimation of Three-Phase Relative Permeability and Residual Oil Data. Journal of Canadian Petroleum Technology. Volume 12. Issue 4. Pages 53 -61.

Tollmann, A. 1976. Analyse des klassischen nordalpinen Mesozoikums (in German). Deuticke. Wien. 580 Pages.

Treiber, L. E. & W. W. Owens. 1972. A Laboratory Evaluation of the Wettability of Fifty Oil-Producing Reservoirs. Society of Petroleum Engineers Journal. Volume 12. Issue 6. Pages 531 – 540.

Ueda, Y., S. Murata, Y. Watanabe & K. Funatsu. 1989. Investigation of the Shape Factor Used in the Dual-Porosity Reservoir Simulator. SPE-19469-MS SPE. Asia-Pacific Conference. 13 - 15 September. Sydney, Australia.

Van Heel, A. P. & P. M. Boerrigter. 2006. On the Shape-Factor in Fractured Reservoir Simulation. SPE Annual Technical Conference and Exhibition. SPE-102471-MS. 24 - 27 September. San Antonio, Texas.

Warren, J. E. & P. J. Root. 1963. The Behavior of Naturally Fractured Reservoirs. Society of Petroleum Engineers Journal. Volume 3. Issue 3. Pages 245 - 255.

World Energy Outlook. 2006. International Energy Agency. Paris, France.

Appendix B

Code for Reference Model

```
RESULTS SIMULATOR IMEX 201210
INUNIT SI
WSRF WELL 1
WSRF GRID TIME
WSRF SECTOR TIME
OUTSRF WELL LAYER NONE
OUTSRF GRID SO SG SW PRES OILPOT BPP SSPRES WINFLUX
WPRN GRID TIME
OUTPRN GRID SO SG SW
OUTPRN RES NONE
RESULTS XOFFSET           0.0000
RESULTS YOFFSET           0.0000
RESULTS ROTATION           0.0000
RESULTS AXES-DIRECTIONS 1.0 -1.0 1.0
GRID VARI 34 34 34
KDIR DOWN
DI IVAR
 0.01 10*0.067 0.01 10*0.067 0.01 10*0.067 0.01
DJ JVAR
 0.01 10*0.067 0.01 10*0.067 0.01 10*0.067 0.01
DK KVAR
 0.01 10*0.067 0.01 10*0.067 0.01 10*0.067 0.01
DTOP
 1156*1000
POR IJK
1:34 1:34 1:34  0.2
1:34 1:34 1:1   0.0015
1:34 1:34 12:12 0.0015
1:34 1:34 23:23 0.0015
1:34 1:34 34:34 0.0015
1:34 1:1 1:34   0.0015
1:34 12:12 1:34 0.0015
1:34 23:23 1:34 0.0015
1:34 34:34 1:34 0.0015
1:1 1:34 1:34   0.0015
```

```
12:12 1:34 1:34 0.0015
23:23 1:34 1:34 0.0015
34:34 1:34 1:34 0.0015
VOLMOD IJK
1:34 1:34 1:1   1.0E+7
1:34 1:34 12:12 1.0E+7
1:34 1:34 23:23 1.0E+7
1:34 1:34 34:34 1.0E+7
1:34 1:1 1:34   1.0E+7
1:34 12:12 1:34 1.0E+7
1:34 23:23 1:34 1.0E+7
1:34 34:34 1:34 1.0E+7
1:1 1:34 1:34   1.0E+7
12:12 1:34 1:34 1.0E+7
23:23 1:34 1:34 1.0E+7
34:34 1:34 1:34 1.0E+7
PERMI CON          10
PERMI IJK
1:34 1:34 1:1   15557
1:34 1:34 12:12 15557
1:34 1:34 23:23 15557
1:34 1:34 34:34 15557
1:34 1:1 1:34   15557
1:34 12:12 1:34 15557
1:34 23:23 1:34 15557
1:34 34:34 1:34 15557
1:1 1:34 1:34   15557
12:12 1:34 1:34 15557
23:23 1:34 1:34 15557
34:34 1:34 1:34 15557
PERMJ CON           10
PERMJ IJK
1:34 1:34 1:1   15557
1:34 1:34 12:12 15557
1:34 1:34 23:23 15557
1:34 1:34 34:34 15557
1:34 1:1 1:34   15557
1:34 12:12 1:34 15557
1:34 23:23 1:34 15557
1:34 34:34 1:34 15557
1:1 1:34 1:34   15557
12:12 1:34 1:34 15557
23:23 1:34 1:34 15557
34:34 1:34 1:34 15557
PERMK CON           10
PERMK IJK
1:34 1:34 1:1   15557
1:34 1:34 12:12 15557
1:34 1:34 23:23 15557
1:34 1:34 34:34 15557
```

```
1:34 1:1 1:34   15557
1:34 12:12 1:34 15557
1:34 23:23 1:34 15557
1:34 34:34 1:34 15557
1:1 1:34 1:34   15557
12:12 1:34 1:34 15557
23:23 1:34 1:34 15557
34:34 1:34 1:34 15557
NULL CON            1
PINCHOUTARRAY CON            1
PRPOR 101.3
CPOR 2.37e-5
MODEL BLACKOIL
TRES 70
PVT EG 1
      101.325  0.678902    1.0455   0.84551   2.54115  0.0124995  4.35113e-006
      527.904   2.08715   1.04838   4.43496   2.40806  0.0125406  4.35113e-006
      954.482   3.69433    1.0517   8.07294   2.27459  0.0125947  4.35113e-006
      1381.06   5.43371   1.05531   11.7597    2.1482  0.0126575  4.35113e-006
      1807.64    7.2747   1.05917   15.4955   2.03107  0.0127275  4.35113e-006
      2234.22   9.19919   1.06324   19.2803   1.92355   0.012804  4.35113e-006
       2660.8   11.1951   1.06749   23.1141   1.82526  0.0128865  4.35113e-006
      3087.37   13.2536    1.0719   26.9967   1.73552  0.0129747  4.35113e-006
      3513.95   15.3682   1.07648   30.9277   1.65354  0.0130683  4.35113e-006
      3940.53   17.5335    1.0812   34.9066   1.57856  0.0131673  4.35113e-006
      4367.11   19.7454   1.08605   38.9328   1.50986  0.0132716  4.35113e-006
      4793.69   22.0003   1.09104   43.0052   1.44678  0.0133811  4.35113e-006
      5220.27   24.2952   1.09616   47.1228   1.38871  0.0134959  4.35113e-006
      5646.84   26.6276   1.10139   51.2843   1.33515  0.0136158  4.35113e-006
      6073.42   28.9953   1.10675   55.4881   1.28561  0.0137408  4.35113e-006
         6500   31.3963   1.11221   59.7322    1.2397   0.013871  4.35113e-006
        12200   66.0479   1.19478   118.923  0.845675  0.0160893  3.55333e-006
        17900   104.252   1.29231    176.37   0.65031  0.0190018  2.16001e-006
        23600   145.045   1.40234   224.994    0.5337  0.0221592  1.50933e-006
        29300    187.91   1.52333   263.695  0.455946    0.02522  1.14038e-006
        35000   232.517   1.65417   294.304  0.400196  0.0280474  9.05894e-007
BWI 1.01501
CVW 0
CW 4.26251e-007
DENSITY OIL 837
DENSITY WATER 1000
REFPW 19620
VWI 0.440258
GRAVITY GAS 0.65
PTYPE CON            1
ROCKFLUID
RPT 1
SWT
 SMOOTHEND POWERQ
          0.2         0         0.3
```

```
        0.225  0.003125    0.263672
         0.25    0.0125    0.229688
        0.275  0.028125    0.198047
          0.3      0.05     0.16875
        0.325  0.078125    0.141797
         0.35    0.1125    0.117187
        0.375  0.153125   0.0949219
          0.4       0.2       0.075
        0.425  0.253125   0.0574219
         0.45    0.3125   0.0421875
        0.475  0.378125   0.0292969
          0.5      0.45     0.01875
        0.525  0.528125   0.0105469
         0.55    0.6125   0.0046875
        0.575  0.703125  0.00117187
          0.6       0.8           0
SLT
          0.4          0.8           0
     0.434375  0.703125333  0.001171875
      0.46875  0.612501333    0.0046875
     0.503125  0.528125333  0.010546875
       0.5375         0.45      0.01875
     0.571875  0.378125333  0.029296875
      0.60625  0.312501333    0.0421875
     0.640625  0.253125067  0.057421875
        0.675          0.2        0.075
     0.709375  0.153125067  0.094921875
      0.74375       0.1125    0.1171875
     0.778125  0.078125067  0.141796875
       0.8125         0.05      0.16875
     0.846875  0.028125067  0.198046875
      0.88125       0.0125    0.2296875
     0.915625  0.003125013  0.263671875
         0.95            0          0.3
RPT 2 OILWET
SWT
 SMOOTHEND POWERQ
            0         0         1
          0.1       0.1       0.9
          0.2       0.2       0.8
          0.3       0.3       0.7
          0.4       0.4       0.6
          0.5       0.5       0.5
          0.6       0.6       0.4
          0.7       0.7       0.3
          0.8       0.8       0.2
          0.9       0.9       0.1
            1         1         0
SLT
            0         1         0
```

```
          0.1       0.9       0.1
          0.2       0.8       0.2
          0.3       0.7       0.3
          0.4       0.6       0.4
          0.5       0.5       0.5
          0.6       0.4       0.6
          0.7       0.3       0.7
          0.8       0.2       0.8
          0.9       0.1       0.9
            1         0         1
RTYPE CON 1
RTYPE IJK
1:34 1:34 1:1   2
1:34 1:34 12:12 2
1:34 1:34 23:23 2
1:34 1:34 34:34 2
1:34 1:1 1:34   2
1:34 12:12 1:34 2
1:34 23:23 1:34 2
1:34 34:34 1:34 2
1:1 1:34 1:34   2
12:12 1:34 1:34 2
23:23 1:34 1:34 2
34:34 1:34 1:34 2
INITIAL
USER_INPUT
PRES CON 20000
SW IJK
1:34 1:34 1:34 0.2
1:34 1:34 1:1   1
1:34 1:34 12:12 1
1:34 1:34 23:23 1
1:34 1:34 34:34 1
1:34 1:1 1:34   1
1:34 12:12 1:34 1
1:34 23:23 1:34 1
1:34 34:34 1:34 1
1:1 1:34 1:34   1
12:12 1:34 1:34 1
23:23 1:34 1:34 1
34:34 1:34 1:34 1
SO IJK
1:34 1:34 1:34 0.8
1:34 1:34 1:1   0
1:34 1:34 12:12 0
1:34 1:34 23:23 0
1:34 1:34 34:34 0
1:34 1:1 1:34   0
1:34 12:12 1:34 0
1:34 23:23 1:34 0
```

```
1:34 34:34 1:34 0
1:1 1:34 1:34   0
12:12 1:34 1:34 0
23:23 1:34 1:34 0
34:34 1:34 1:34 0
PB CON         10000
NUMERICAL
RUN
DATE 2015  1  1
DATE 2015  1  6
DATE 2015  1 11
DATE 2015  1 16
DATE 2015  1 21
DATE 2015  1 26
DATE 2015  1 31
DATE 2015  2  5
DATE 2015  2 10
DATE 2015  2 15
DATE 2015  2 20
DATE 2015  2 25
DATE 2015  3  2
DATE 2015  3  7
DATE 2015  3 12
DATE 2015  3 17
DATE 2015  3 22
DATE 2015  3 27
DATE 2015  4  1
DATE 2015  4  6
DATE 2015  4 11
DATE 2015  4 16
DATE 2015  4 21
DATE 2015  4 26
DATE 2015  5  1
DATE 2015  5  6
DATE 2015  5 11
DATE 2015  5 16
DATE 2015  5 21
DATE 2015  5 26
DATE 2015  5 31
DATE 2015  6  5
DATE 2015  6 10
DATE 2015  6 15
DATE 2015  6 20
DATE 2015  6 25
DATE 2015  6 30
STOP
RESULTS RELPERMCORR NUMROCKTYPE 1
RESULTS RELPERMCORR CORRVALS 0.2 0.2 0.4 0.4 0.2 0.2 0.05 0.05
RESULTS RELPERMCORR CORRVALS 0.8 0.3 0.3 0.8 2 2 2 2
RESULTS RELPERMCORR CORRVALS_HONARPOUR -99999 -99999 -99999 -99999
```

```
-99999 -99999 -99999 -99999
RESULTS RELPERMCORR NOSWC false
RESULTS RELPERMCORR CALINDEX  0
RESULTS RELPERMCORR STOP
RESULTS SPEC 'PVT Type'
RESULTS SPEC SPECNOTCALCVAL -99999
RESULTS SPEC REGION 'All Layers (Whole Grid)'
RESULTS SPEC REGIONTYPE 'REGION_WHOLEGRID'
RESULTS SPEC LAYERNUMB 0
RESULTS SPEC PORTYPE 1
RESULTS SPEC CON 1
RESULTS SPEC SPECKEEPMOD 'YES'
RESULTS SPEC STOP
RESULTS SPEC 'Bubble Point Pressure'
RESULTS SPEC SPECNOTCALCVAL -99999
RESULTS SPEC REGION 'PVT Type 1'
RESULTS SPEC REGIONTYPE 'REGION_TABLE'
RESULTS SPEC LAYERNUMB 1
RESULTS SPEC PORTYPE 1
RESULTS SPEC CON 6500
RESULTS SPEC SPECKEEPMOD 'YES'
RESULTS SPEC STOP
RESULTS SPEC 'Permeability I'
RESULTS SPEC SPECNOTCALCVAL -99999
RESULTS SPEC REGION 'All Layers (Whole Grid)'
RESULTS SPEC REGIONTYPE 'REGION_WHOLEGRID'
RESULTS SPEC LAYERNUMB 0
RESULTS SPEC PORTYPE 1
RESULTS SPEC CON 10
RESULTS SPEC SPECKEEPMOD 'YES'
RESULTS SPEC STOP
RESULTS SPEC 'Grid Thickness'
RESULTS SPEC SPECNOTCALCVAL -99999
RESULTS SPEC REGION 'All Layers (Whole Grid)'
RESULTS SPEC REGIONTYPE 'REGION_WHOLEGRID'
RESULTS SPEC LAYERNUMB 0
RESULTS SPEC PORTYPE 1
RESULTS SPEC CON 1.5
RESULTS SPEC SPECKEEPMOD 'YES'
RESULTS SPEC STOP
RESULTS SPEC 'Grid Top'
RESULTS SPEC SPECNOTCALCVAL -99999
RESULTS SPEC REGION 'Layer 1 - Whole layer'
RESULTS SPEC REGIONTYPE 'REGION_LAYER'
RESULTS SPEC LAYERNUMB 1
RESULTS SPEC PORTYPE 1
RESULTS SPEC CON 1000
RESULTS SPEC SPECKEEPMOD 'YES'
RESULTS SPEC STOP
```